Kondo Interactions from Band Reconstruction in $YbInCu_4$

I. Jarrige,[1,*] A. Kotani,[2] H. Yamaoka,[3] N. Tsujii,[4] K. Ishii,[5] M. Upton,[6] D. Casa,[6] J. Kim,[6] T. Gog,[6] and J. N. Hancock[7]
[1]National Synchrotron Light Source II, Brookhaven National Laboratory, Upton, New York 11973-5000, USA
[2]Photon Factory, Institute of Materials Structure Science, High Energy Accelerator Research Organization, 1-1 Oho, Tsukuba, Ibaraki 305-0801, Japan
[3]RIKEN SPring-8 Center, Sayo, Hyogo 679-5148, Japan
[4]Quantum Beam Center, National Institute for Materials Science, 1-2-1 Sengen, Tsukuba 305-0047, Japan
[5]Japan Atomic Energy Agency, SPring-8, Sayo, Hyogo 679-5148, Japan
[6]Advanced Photon Source, Argonne National Laboratory, Argonne, Illinois 60439, USA
[7]Department of Physics and Institute for Materials Science, University of Connecticut, Storrs, Connecticut 06269, USA
(Received 18 August 2014; revised manuscript received 5 January 2015; published 27 March 2015)

We combine resonant inelastic x-ray scattering and model calculations in the Kondo lattice compound $YbInCu_4$, a system characterized by a dramatic increase in Kondo temperature and associated valence fluctuations below a first-order valence transition at $T \simeq 42$ K. The bulk-sensitive, element-specific, and valence-projected charge excitation spectra reveal an unusual quasigap in the Yb-derived state density which drives an instability of the electronic structure and renormalizes the low-energy effective Hamiltonian at the transition. Our results provide long-sought experimental evidence for a link between temperature-driven changes in the low-energy Kondo scale and the higher-energy electronic structure of this system.

DOI: 10.1103/PhysRevLett.114.126401 PACS numbers: 71.20.Eh, 72.15.Qm, 75.20.Hr, 78.70.Ck

The first-order isostructural valence transition in $YbInCu_4$ is one of the most intriguing localization-delocalization problems in correlated electron systems. Unlike model impurity systems and many Kondo lattice materials which are characterized by a single Kondo temperature T_K, $YbInCu_4$ undergoes a dramatic steplike increase of the Kondo coupling scale from $T_K = 25$ to $T_K = 400$ K upon cooling below 42 K with associated changes in the Yb valence (2.96 to 2.83) [1,2], pointing to an anomalous increase in screening of the local moment sublattice. While valence transitions in f electron systems can usually be explained on the basis of either of two possible theoretical approaches, the Kondo volume collapse (KVC) and the Mott transition, no such conclusive theoretical interpretation has yet been advanced for the transition in $YbInCu_4$. The strong coupling between volume and T_K assumed in the KVC is not supported by the relatively small value reported for the appropriate Gruneisen parameter [3,4], and the Mott transition scenario is ruled out by the 0.5% increase in the volume at the transition [5]. A different theoretical approach attributes the enhancement of the Kondo coupling at the transition to a larger exchange interaction between the f and conduction-band electron spins resulting from an increase of the Coulomb interaction [6].

During the past decade, a number of spectroscopic measurements have added valuable pieces to the puzzle of the nature of the electronic phase transition. Fine measurements of the Yb valence, enabled by the emergence of advanced hard x-ray core-level spectroscopies like resonant x-ray emission spectroscopy [2], hard x-ray photoelectron spectroscopy [7], and x-ray absorption spectroscopy (XAS) in the partial fluorescence yield mode [8] highlight the sensitivity of x-ray probes to the valence transition in this system. Meanwhile, using softer photons, optical conductivity measurements revealed a midinfrared peak associated with the Kondo resonance below T_K [9–12], which appears to be a universal trait of Kondo lattice and heavy fermion systems. On the other hand, while detailed knowledge of the electronic structure is essential to understanding valence transitions [13,14], the high electronic dimensionality and known surface sensitivity in mixed valence systems limit the effectiveness of traditional approaches [2,12,15,16] to probing the electronic structure of $YbInCu_4$.

In order to fill this gap in our understanding, we used resonant inelastic x-ray scattering (RIXS), a bulk-sensitive, orbital, and element-selective probe of the electronic structure to explore the changes in low-energy states while crossing the valence transition. RIXS is a Raman process which generates low-lying excitations through resonant x-ray edge intermediate states of well-defined orbital character. In our measurements at the Yb-L_3 edge, a $2p$ core electron is photoexcited into a valence state of d character, followed by decay of a d-character valence electron into the core hole [17]. The nascent presence of the $2p$ core hole potential induces excitations among rare-earth $5d$ states, which are forbidden through direct dipole transitions relevant to optical conductivity. Here we observe several intense RIXS-active excitations, and use the valence selectivity of RIXS to uncover temperature-driven spectral changes up to several eV. These changes trend with an

energy shift of itinerant $5d$ states, revealing the energetics of an underlying instability driving the transition.

Our experiments were performed at the MERIX end station of the XOR-IXS 30-ID beam line at the Advanced Photon Source [18]. Single crystals of $YbInCu_4$ were grown using the flux method and cleaved [12] before measurement with crystal facet along (111). $YbInCu_4$ has the cubic $C15b$ ($AuBe_5$ type) structure [19]. The horizontally polarized incident beam was monochromatized using a four-bounce scheme of asymmetrically cut Si(400) crystals, scattered from the sample, and energy analyzed with a 4-in. diameter diced Ge (008) spherical analyzer and a strip detector placed on a 1-m Rowland spectrometer. A resultant energy resolution of 0.2 eV was achieved in the horizontal scattering geometry, with a scattering angle of 90° and momentum transfer $Q = (5.5, 3.5, 3.5)$ indexed to the cubic unit cell, which contains 4 f.u.

Figures 1(a) and 1(b) show the XAS spectra as a white curve superimposed over the Yb L_3 RIXS planes for the high-temperature (HT, 70 K) and low-temperature (LT, 35 K) phases, respectively. The HT XAS spectrum displays prominent structures at 8961 and 8965 eV, which represent core-hole containing final states (RIXS intermediate states) with mainly $4f^{13}$ electron configuration (Yb^{3+}) [20,21]. In the LT phase, an additional shoulder emerges at a lower energy of 8953 eV and contains mainly $4f^{14}$ character (Yb^{2+}). The strong core hole potential is responsible for the reversal of energy ordering of these valence configurations relative to the lower energy (<10 eV) manifold. The excited core hole has many possible decay channels, one of which is the spectrally resolved RIXS process. As indicated by the arrow in Fig. 1(b), a RIXS-active excitation around 3 eV strengthens when the incident energy is tuned near the Yb^{2+} feature in the LT phase. Figure 1(c) displays the intensity difference between the LT and HT RIXS planes of Figs. 1(b) and 1(a), highlighting additional changes in the < 10 eV range, and revealing that scattering through the Yb^{3+} and Yb^{2+} resonances evolves in opposite ways across the valence transition.

To better understand the nature of the observed spectra, the incident energy dependent RIXS spectrum was calculated using the single-impurity Anderson model (SIAM) [21–23] and is shown for the LT phase in Fig. 1(d). The remarkable agreement with the experimental data of Fig. 1(b) was achieved using a detailed bare band structure of the Yb d density of states (DOS) [20] which was calculated within the local-spin density approximation and includes on-site $4f$ Coulomb interaction (LSDA + U), and is reproduced as a histogram in Fig. 2(a). Figure 2(b) depicts the radiative transitions for the XAS and RIXS processes in the many-body SIAM [21]. The green rectangles represent the unoccupied part of the ligand band corresponding to the continuum of transitions between the multielectronic $4f^{14}$ and $4f^{13}c$ levels, where c is an electron transferred to the ligand band. The RIXS intermediate and final state configurations, respectively, have a

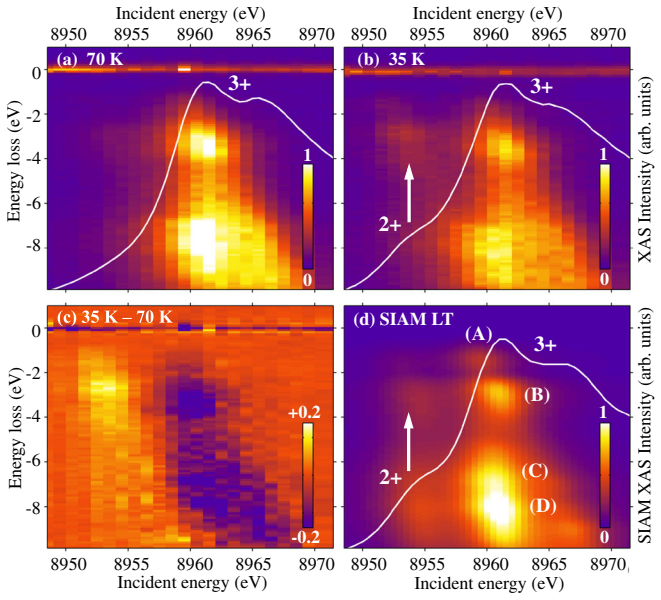

FIG. 1 (color online). Color plot of the Yb-L_3 RIXS plane with the absorption spectrum (solid white line) measured at (a) 70 and (b) 35 K, and (d) calculated for the LT phase using the SIAM and scaled to the experimental intensity. (c) The difference between the spectra measured at 35 and 70 K. The excitation labels (A), (B), (C), (D) correspond to the transitions in Fig. 2(a).

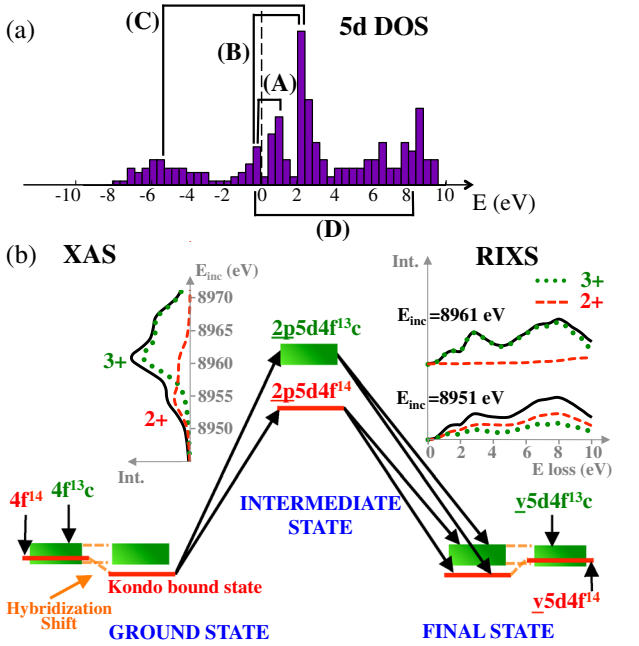

FIG. 2 (color online). (a) Band diagram showing the occupied and unoccupied Yb d DOS used in the SIAM and the transitions assigned to RIXS peaks. (b) Total energy level scheme for a mixed-valence Yb ion, with radiative transitions in the SIAM and calculated RIXS and XAS spectral functions and their Yb^{2+} and Yb^{3+} components.

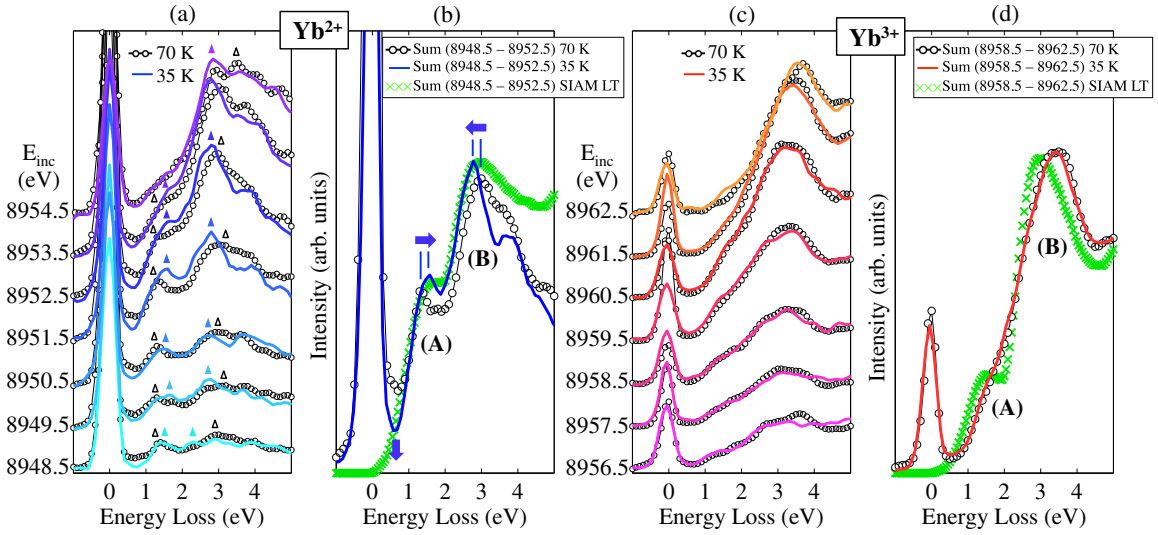

FIG. 3 (color online). Incident energy resolved RIXS profile measured at 35 and 70 K across the 8948.5–8952.5 eV (a) and 8958.5–8962.5 eV (c) incident energy ranges, which, respectively, correspond to the Yb^{2+} and Yb^{3+} components in the LT XAS spectrum. In (a), the filled and open triangles indicate the peak position of (*A*) and (*B*) at 35 and 70 K, respectively. The Yb^{3+} spectra in (c) are intensity scaled by 0.4 for comparison with Yb^{2+} in (a), and for each incident energy the HT spectra are normalized to the area of the LT spectra over the 0.5–5.0 eV range to ease the comparison between the low-energy features. The raw RIXS spectra averaged over these respective incident energy ranges are shown in (b) and (d) along with the corresponding calculated spectra for the LT phase. In (b), the arrows indicate the direction of variations in the RIXS intensity upon cooling from 70 to 35 K.

hole in the $2p$ level and in the $5d$ valence band, and there are four transition paths allowed [24]. The calculated RIXS spectral functions in Fig. 2(b) explicitly illustrate the tunable valence state selectivity through the incident energy dependence of the RIXS cross section. The SIAM is explained in more detail in Ref. [25].

The agreement between the panels Figs. 1(b) and 1(d) permits assignment of the salient spectral features to specific electronic transitions among Yb $5d$ occupied and unoccupied states [see Fig. 2(a)]. The RIXS process responsible for the small structure labeled (*A*) at ~1.5 eV involves photoexcitation of a core electron into the shoulder of the unoccupied $5d$ DOS around 1.5 eV above the Fermi level E_F, followed by coherent recombination of an electron from the $5d$ peak just below E_F into the core hole. A second, stronger feature centered around 3 eV, and two higher-energy excitations in the 6–10 eV range correspond, respectively, to the transitions signified by the lines labeled (*B*), (*C*), and (*D*) in Fig. 2(a).

We now show that the valence-selective nature of the RIXS probe provides unique insight into the dependence of the low-energy charge excitations on the f shell occupancy. Figures 3(a) and 3(c), respectively, show the incident-energy resolved RIXS spectra separately for the energy ranges corresponding to the Yb^{2+} (8948.5–8952.5 eV) and Yb^{3+} (8958.5–8962.5 eV) components in the LT XAS spectrum. To simplify presentation, these RIXS spectra were averaged over the energy windows around each intermediate valence state and are shown in Figs. 3(b) and 3(d), respectively, along with the corresponding SIAM summed intensity for the LT phase. Upon cooling across the transition, the spectra for the Yb^{3+} intermediate states show only weak changes, while those for the Yb^{2+} intermediate states reveal dramatic reconstruction, with a quasigap-like dip opening around 0.5 eV, and the shifts of the features (*A*) and (*B*) by, respectively, +0.2 and −0.2 eV.

The RIXS-enabled selectivity of excitations related to the divalent state reveals an unprecedentedly clear view of the temperature-induced changes in Yb $5d$ states. In the LT phase, the Yb mean valence drops to 2.83 and an XAS shoulder related to Yb^{2+} appears [see Fig. 1(b)]. An attempt to understand the dependence of charge excitations on f occupancy was made in the context of optical spectra [20], where calculations within the LSDA + U and LSDA approximations yielded f counts of nearly 13 (Yb^{3+}) and 14 (Yb^{2+}), respectively, and a virtual crystal variant of the LSDA + U covered intermediate valence cases of $Yb^{2.8+}$ and $Yb^{2.9+}$. For the increased f count, mimicking the LT phase, more effective screening of the Yb nuclear charge was found to cause a shift of the empty on-site Yb $5d$ band upwards towards lower binding energies, while off-site electronic states derived from high binding energy In $5p$ states are less sensitive to changes in screening efficiency. This effect was suggested to explain valence transition-induced shift observed in a set of In $5p \rightarrow$ Yb $5d$ interband transitions which strongly resemble feature (*A*) in our RIXS spectra. The similar absolute energy, magnitude, and sign of the shift of the optical transitions and feature (*A*) suggests that the nuclear screening effect is also manifest in the Yb $5d \rightarrow$ Yb $5d$ RIXS interband transitions.

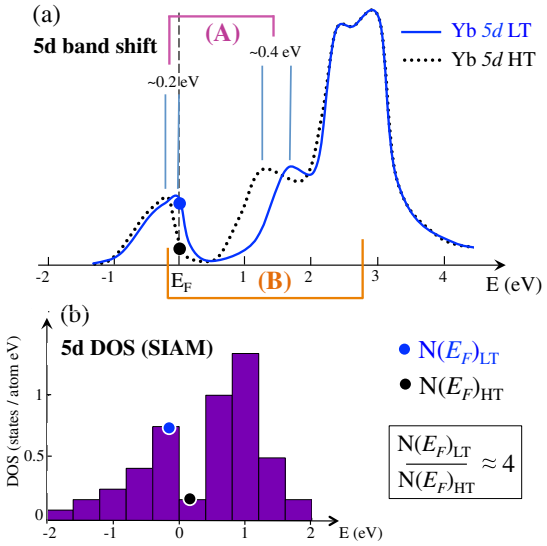

FIG. 4 (color online). (a) Schematic illustration of the nonrigid shift of the Yb $5d$ band across the transition. The shift towards lower binding energies is about twice for the shoulder in the unoccupied states around 1.5 eV than for the occupied states, as inferred from the 0.2 eV blueshift of (A) and 0.2 eV redshift of (B) in the RIXS data. (b) The Fermi level moves out of the quasigap while the Yb $5d$ Fermi DOS [Fig. 2(a)] sharply increases at LT.

Feature (B) was not observed in optical conductivity and is *redshifted* by 0.2 eV in the LT-RIXS spectrum. The opposite temperature-dependent behavior of the features (A) and (B) coupled with our convincing assignment of these features within the LT phase shown in Figs. 1(b) and 1(d) imply that a rigid-shift picture of the Yb $5d$ band breaks down across the transition. While further theoretical treatment is appropriate to better understand the detailed cause-effect connections between nuclear screening, f count, and the observed electronic structure changes, here we explore possible influences on the nonrigid $5d$ band, as schematically illustrated in Fig. 4(a). Optical conductivity measurements have revealed a sharp midinfrared peak associated with Kondo resonance formation below T_K [10–12], ascribed to dipole-active transitions across the correlation-induced gap between hybridized bands near E_F. We speculate that the formation of these hybridized bands may play a role in partially pinning the $5d$ states located around E_F due to the more effective mixing with the $4f$-hybridizing In $5p$ states at higher binding energy, and that the portion of the unoccupied $5d$ band at lower binding energy is less sensitive to changes in screening efficiency. While the detailed origin of these marked spectral changes requires advanced theoretical methods such as dynamical mean field theory, our experimental exploration of the partial DOS enabled by RIXS gives a new window into the electronic structure of this and other strongly correlated electron systems.

We now turn to the quasigap observed around 0.5 eV in Fig. 3(b), and its relation with the quasigap in the DOS around E_F [20,27]. As illustrated in Fig. 4(a), the shift of the Yb $5d$ occupied and unoccupied bands towards lower binding energies is expected to push the quasigap away from the Fermi level. To estimate the effect on parameters relevant to the macroscopic material behavior, we use the observed shift ~0.2 eV and calculated Yb $5d$ DOS to estimate $N(E_F)_{\mathrm{LT}}/N(E_F)_{\mathrm{HT}} \approx 4$ as a rough fractional change in $5d$ Fermi DOS upon cooling through the transition [see Fig. 4(b)]. This is consistent with the jump in the carrier concentration observed below the transition [5] and the observed lowering of RIXS intensity in this spectral region, and would cause the abrupt rise of T_K at LT, as discussed below. A link between a subtle change in the position of the DOS quasigap with respect to E_F and the transition had been previously hypothesized on the basis of Hall effect [28] and Cu-$2p_{3/2}$ XAS spectra [29], and our results provide direct evidence for this relationship.

Within the SIAM, T_K can be expressed as $k_B T_K = [(1-n_h)/n_h] N_f \tilde{V}^2$, where $\tilde{V}^2 = \rho(E_F) V^2$, n_h is the number of $4f$ holes and N_f is the degeneracy of the $4f$ states. $\rho(E_F)$ is the partial DOS of the relevant ligand band, which is primarily derived from extended In $5p$ orbitals. Yb $5d$ and In $5p$ bands have dominant contributions to the carrier concentration and are expected to be strongly hybridized with each other due to their large orbital extent and close physical proximity, a fact supported by the similarities between these partial DOS in energy band calculations [20,27]. To estimate the DOS effect on T_K, we assume that the strong correlation between the Yb $5d$ DOS $\mathrm{N}(E_F)$ and ligand DOS $\rho(E_F)$ is such that a variation in $N(E_F)$ gives rise to a proportional variation in $\rho(E_F)$. Under this assumption, the ratio $\rho(E_F)_{\mathrm{LT}}/\rho(E_F)_{\mathrm{HT}}$ is approximately the same as $N(E_F)_{\mathrm{LT}}/N(E_F)_{\mathrm{HT}}$, ~4. In fact, using the experimentally derived values of n_h and T_K [1,2] in the above expression of T_K, one estimates $[V^2\rho(E_F)]_{\mathrm{LT}}/[V^2\rho(E_F)]_{\mathrm{HT}} = 3.2$, which is reasonably close to our estimation of $\rho(E_F)_{\mathrm{LT}}/\rho(E_F)_{\mathrm{HT}}$, suggesting that the first-order change in T_K is largely due to the jump in DOS at E_F, in stark contrast to the phenomenologically similar γ-α transition in Ce, which is usually interpreted in terms of a volume-induced change of V [30]. We also note that related systems $YbInCu_5$ [31] and $YbAgCu_4$ [5] show continuous valence crossover behavior, and have relatively smooth and quasigap-free near-E_F DOS profiles, bolstering the key role of the strongly indented profile of the DOS around E_F in the anomalous first-order transition in $YbInCu_4$.

We have carried out RIXS measurements of $YbInCu_4$ across the isostructural valence transition, which show pronounced electronic structure changes, particularly for excitations derived from divalent intermediate states. These changes indicate that the Fermi level migrates out of an unusual quasigap following the onset of the mixed-valence

behavior at LT. The striking rise of T_K below the transition is a result of sharp contrast in the energy-dependent state density near the Fermi level, a condition which is left out of common theoretical considerations of the Kondo effect. These results establish a link between the bare band structure and the Kondo scale at the heart of the valence transition and suggest a roadmap for identifying materials with temperature-driven valence transitions, and the associated reversible magnetocaloric effect [32] closer to room temperature, enabling compressor-free refrigeration for a sustainable energy future. Further, through a novel application of RIXS, we have clearly demonstrated how the valence sensitivity of this emerging spectroscopic technique can disclose subtle changes in electronic structure to reveal new physics in the context of Kondo interactions.

We thank T. Fukuda for his help with aligning the single crystal. Use of the APS, an Office of Science User Facility operated for the US DOE Office of Science by Argonne National Laboratory, was supported by the US DOE under Contract No. DE-AC02-06CH11357.

*To whom correspondence should be addressed: E-mail: jarrige@bnl.gov

[1] J. L. Sarrao, C. D. Immer, C. L. Benton, Z. Fisk, J. M. Lawrence, D. Mandrus, and J. D. Thompson, Phys. Rev. B **54**, 12207 (1996).
[2] C. Dallera, M. Grioni, A. Shukla, G. Vankó, J. L. Sarrao, J. P. Rueff, and D. L. Cox, Phys. Rev. Lett. **88**, 196403 (2002).
[3] A. Yu Sokolov, H. Nakamura, and M. Shiga, J. Phys. Condens. Matter **11**, 6463 (1999).
[4] J. L. Sarrao, A. P. Ramirez, T. W. Darling, F. Freibert, A. Migliori, C. D. Immer, Z. Fisk, and Y. Uwatoko, Phys. Rev. B **58**, 409 (1998).
[5] A. L. Cornelius, J. M. Lawrence, J. L. Sarrao, Z. Fisk, M. F. Hundley, G. H. Kwei, J. D. Thompson, C. H. Booth, and F. Bridges, Phys. Rev. B **56**, 7993 (1997).
[6] A. V. Goltsev and G. Bruls, Phys. Rev. B **63**, 155109 (2001).
[7] H. Sato, K. Shimada, M. Arita, K. Hiraoka, K. Kojima, Y. Takeda, K. Yoshikawa, M. Sawada, M. Nakatake, H. Namatame, M. Taniguchi, Y. Takata, E. Ikenaga, S. Shin, K. Kobayashi, K. Tamasaku, Y. Nishino, D. Miwa, M. Yabashi, and T. Ishikawa, Phys. Rev. Lett. **93**, 246404 (2004).
[8] H. Yamaoka, N. Tsujii, K. Yamamoto, A. M. Vlaicu, H. Oohashi, H. Yoshikawa, T. Tochio, Y. Ito, A. Chainani, and S. Shin, Phys. Rev. B **78**, 045127 (2008).
[9] S. R. Garner, J. N. Hancock, Y. W. Rodriguez, Z. Schlesinger, B. Bucher, Z. Fisk, and J. L. Sarrao, Phys. Rev. B **62**, R4778 (2000).
[10] J. N. Hancock, T. McKnew, Z. Schlesinger, J. L. Sarrao, and Z. Fisk, Phys. Rev. Lett. **92**, 186405 (2004).
[11] J. N. Hancock, T. McKnew, Z. Schlesinger, J. L. Sarrao, and Z. Fisk, Phys. Rev. B **73**, 125119 (2006).
[12] H. Okamura, T. Michizawa, T. Nanba, and T. Ebihara, Phys. Rev. B **75**, 041101(R) (2007).
[13] P. Strange, A. Svane, W. M. Temmerman, Z. Szotek, and H. Winter, Nature (London) **399**, 756 (1999).
[14] W. M. Temmerman, A. Svane, L. Petit, M. Luders, P. Strange, and Z. Szotek, Phase Transit. **80**, 415 (2007).
[15] F. Reinert, R. Claessen, G. Nicolay, D. Ehm, S. Hüfner, W. P. Ellis, G.-H. Gweon, J. W. Allen, B. Kindler, and W. Assmus, Phys. Rev. B **58**, 12808 (1998).
[16] D. P. Moore, J. J. Joyce, A. J. Arko, J. L. Sarrao, L. Morales, H. Hochst, and Y. D. Chuang, Phys. Rev. B **62**, 16492 (2000).
[17] A. Kotani, K. O. Kvashnina, S. M. Butorin, and P. Glatzel, Eur. Phys. J. B **85**, 257 (2012).
[18] Y. Shvyd'ko, J. Hill, C. Burns, D. Coburn, B. Brajuskovic, D. Casa, K. Goetze, T. Gog, R. Khachatryan, J.-H. Kim, C. Kodituwakku, M. Ramanathan, T. Roberts, A. Said, H. Sinn, D. Shu, S. Stoupin, M. Upton, M. Wieczorek, and H. Yavas, J. Electron Spectrosc. Relat. Phenom. **188**, 140 (2013).
[19] J. M. Lawrence, G. H. Kwei, J. L. Sarrao, Z. Fisk, D. Mandrus, and J. D. Thompson, Phys. Rev. B **54**, 6011 (1996).
[20] V. N. Antonov, M. Galli, F. Marabelli, A. N. Yaresko, A. Ya. Perlov, and E. Bauer, Phys. Rev. B **62**, 1742 (2000).
[21] A. Kotani, Eur. Phys. J. B **85**, 31 (2012).
[22] A. Kotani, K. O. Kvashnina, P. Glatzel, J. C. Parlebas, and G. Schmerber, Phys. Rev. Lett. **108**, 036403 (2012).
[23] A. Kotani, Mod. Phys. Lett. B **27**, 1330012 (2013).
[24] We note that the model is set to simulate the so-called direct RIXS process as described in Ref. [17], which consists of an excitation from the core level $2p$ to an empty $5d$ state in the intermediate state followed by the filling of the $2p$ core hole by an electron from an occupied $5d$ state in the final state. The so-called indirect RIXS process, which occurs via a shake-up of the electronic system in the presence of the core hole, is forbidden for a scattering angle of 90° [17], which we used in the experiment, and is therefore not included in the model.
[25] See Supplemental Material at http://link.aps.org/supplemental/10.1103/PhysRevLett.114.126401, which includes Ref. [26], for detailed description of the single impurity Anderson model (SIAM) used in this study, and additional comparison between the model and the experimental data.
[26] O. Gunnarsson and K. Schönhammer, Phys. Rev. B **28**, 4315 (1983).
[27] K. Takehagara and T. Kasuya, J. Phys. Soc. Jpn. **59**, 3299 (1990).
[28] E. Figueroa, J. M. Lawrence, J. L. Sarrao, Z. Fisk, M. F. Hundley, and J. D. Thompson, Solid State Commun. **106**, 347 (1998).
[29] Y. Utsumi, H. Sato, H. Kurihara, H. Maso, K. Hiraoka, K. Kojima, K. Tobimatsu, T. Ohkochi, S.-i. Fujimori, Y. Takeda, Y. Saitoh, K. Mimura, S. Ueda, Y. Yamashita, H. Yoshikawa, K. Kobayashi, T. Oguchi, K. Shimada, H. Namatame, and M. Taniguchi, Phys. Rev. B **84**, 115143 (2011).
[30] See, for instance, K. Haule, V. Oudovenko, S. Y. Savrasov, and G. Kotliar, Phys. Rev. Lett. **94**, 036401 (2005).
[31] H. Yamaoka, I. Jarrige, N. Tsujii, N. Hiraoka, H. Ishii, and K.-D. Tsuei, Phys. Rev. B **80**, 035120 (2009).
[32] A. L. Lima Sharma, A. M. Gomes, C. Salazar Mejia, F. R. Drymiotis, and A. M. G. Carvalho, J. Appl. Phys. **108**, 083918 (2010).

Supplementary Material: Kondo interactions from band reconstruction in $YbInCu_4$

We calculate the RIXS spectra in the low temperature phase of $YbInCu_4$ using a single impurity Anderson model (SIAM). The present SIAM is very similar to that used by Kotani[S1], although here we reformulate it using the electron picture instead of the hole picture in Ref. S1. The method of calculating RIXS with SIAM is similar to what was described in Refs. [S2–S4], where RIXS was calculated for mixed-valence Ce compounds, but here we apply the model to the calculation of RIXS for $YbInCu_4$.

The SIAM consists of the Yb $4f$, $5d$ and $2p_{3/2}$ states on a single Yb site and a ligand band which hybridizes with the Yb $4f$ states. The ligand band mainly corresponds to the In $5p$ states, and here we treat it, for simplicity, as a half-filled band with the density of states (DOS) of rectangular shape (the half-width of the band is denoted by W). The DOS of the Yb $5d$ states is shown in Fig. 2(a), which is simulated from the results of the energy band calculations by Antonov *et al.*[S5] The $5d$ electrons are treated as free electrons with no interaction with the other electrons.

The ground state of our system is given by a linear combination of the two configurations, $4f^{14}$ and $4f^{13}c$ (c representing a ligand electron), in the following form:

$$|g\rangle = c_0^{(g)}|4f^{14}\rangle + \sum_{k,j_z} c_{k,j_z}^{(g)}|k,j,j_z\rangle, \tag{S1}$$

where $|4f^{14}\rangle$ is the many-body state expressed as

$$|4f^{14}\rangle = \prod_{j,j_z} f_{j,j_z}^{\dagger}|0\rangle \tag{S2}$$

and $|k,j,j_z\rangle$ is given by

$$|k,j,j_z\rangle = a_{k,j_z}^{\dagger} f_{j,j_z}|4f^{14}\rangle. \tag{S3}$$

Here, $f_{j,j_z}^{\dagger}$ and f_{j,j_z} are the creation and annihilation operators of the $4f$ electron with angular momentum (j,j_z), $|0\rangle$ is the state where the ligand and $5d$ band states below the Fermi level are all occupied, and $a_{k,j_z}^{\dagger}$ is the creation operator of a ligand electron (k being the index representing the energy of the ligand electron). In $|k,j,j_z\rangle$ we fix $j=5/2$. The states $|4f^{14}\rangle$ and $|k,j,j_z\rangle$ are coupled by hybridization V. The expression (1) corresponds to the ground state in the lowest order approximation of the $1/N_f$ expansion method[S6] and in the limit of the infinite Coulomb interaction between $4f$ electrons, where N_f is the degeneracy of the $4f$ states.

As illustrated in Fig. 2(b), the $4f^{14}$ configuration (the state$|4f^{14}\rangle$) has a single energy level (denoted by $E(4f^{14})$ shown by a red line and the $4f^{13}c$ configuration (each of the $|k,j,j_z\rangle$ state) has a continuous energy band shown by a green rectangle. The energy of $|k,j,j_z\rangle$ is expressed as $E(4f^{14})+\epsilon_k-\epsilon_f$, where $\epsilon_k-\epsilon_f$ is the energy change by transferring a $4f(j=5/2)$ electron to the ligand band (with energy ϵ_k) above the Fermi level. By switching on the hybridization, the two configurations are mixed with each other and a bound state (Kondo bound state) is formed below the energy continuum. There are three parameters, $\tilde{V}$, ϵ_f and W, to describe the ground state of our SIAM, where $\tilde{V}^2=\rho(E_F)V^2$ with $\rho(E_F)$ being the DOS of the ligand band. We take $\tilde{V}$=0.322 eV, ϵ_f=-0.768 eV, and W=2.0 eV, so as to reproduce the valence v=2.83 and the Kondo temperature T_K=480 K. For the relations among V, ϵ_f, W, v and T_K, see Ref.1.

By an incident photon with energy Ω, a $2p_{3/2}$ core electron with energy $\epsilon_{2p_{3/2}}$ is excited to the Yb $5d$ band (with energy $\epsilon_{5d_{k_e}}$) above the Fermi energy. This is an intermediate state of RIXS (and also a final state of XAS). We have two configurations, $\underline{2p}5d4f^{14}$ and $\underline{2p}5d4f^{13}c$, which are hybridized by V. We take into account that the attractive core-hole potential -U_{fc} (= -7 eV) acts on the $4f$ electron, so that the energy of the $\underline{2p}5d4f^{14}$ configuration becomes much lower than the $\underline{2p}5d4f^{13}c$, as shown in Fig. 2(b). Therefore, the mixing of the two configurations becomes very small, and disregarded in Fig. 2(b). In our numerical calculation, we take into account the small hybridization effect, and describe each intermediate state of RIXS in the form:

$$|m_{k_e,i}\rangle = d_{k_e}^{\dagger}p_{3/2}|i\rangle = d_{k_e}^{\dagger}p_{3/2}\{c_0^{(i)}|4f^{14}\rangle + \sum_{k,j_z} c_{k,j_z}^{(i)}|k,j,j_z\rangle\}, \tag{S4}$$

where $d_{k_e}^{\dagger}$ and $p_{3/2}$ represent the creation of the $5d$ electron and the annihilation of the $2p_{3/2}$ electron, respectively. Now the energies of $|4f^{14}\rangle$ and $|k,j,j_z\rangle$ are $E(4f^{14})$ and $E(4f^{14})+\epsilon_k-\epsilon_f-U_{fc}$, respectively.

The XAS spectrum is given by

$$F_{\rm XAS}(\Omega) = \sum_{k_e,i} |\langle m_{k_e,i}|M|g\rangle|^2 \frac{\Gamma/\pi}{(\Omega - E_{k_e,i} + E_g)^2 + \Gamma^2}, \tag{S5}$$

where Γ is the spectral broadening due to the lifetime of the $2p_{3/2}$ core hole, and $E_{k_e,i}(=\epsilon_{5d_{k_e}}-\epsilon_{2p_{3/2}}+E_i)$ and E_g are the energies of the states $|m_{k_e,i}\rangle$ and $|g\rangle$, respectively, and M is the one-electron dipole-transition operator for the $2p$ to $5d$ excitation.

In the final state of RIXS, a $5d$ electron (with energy ϵ_{k_v}) below the Fermi level makes a dipole transition to the $2p_{3/2}$ core state. Therefore, we have two configurations, $\underline{v}5d4f^{14}$ and $\underline{v}5d4f^{13}c$, and each final state is written as

$$|f_{k_e,k_v,i'}\rangle = d_{k_e}^{\dagger}d_{k_v}|i'\rangle, \tag{S6}$$

where $|i'\rangle$ is given by

$$|i'\rangle = c_0^{(i')}|4f^{14}\rangle + \sum_{k,j_z} c_{k,j_z}^{(i')}|k,j,j_z\rangle. \tag{S7}$$

It is to be noted that the hybridization between $|4f^{14}\rangle$ and $|k,j,j_z\rangle$ in $|i'\rangle$ is exactly the same as that for the ground state $|g\rangle$. Actually, the lowest state of $|i'\rangle$ is the

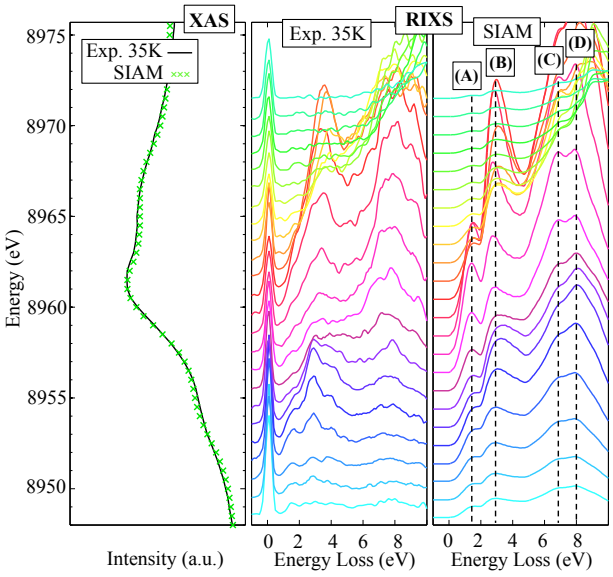

FIG. S1. (Color online) (left panel) Yb-L_3 XAS spectrum measured at 35 K and calculated for the LT phase using the SIAM. Incident energy dependence of the RIXS spectra measured at 35 K (middle panel) and calculated for the LT phase using the SIAM (right panel). The vertical dashed lines indicate the position of the four main excitations in the calculated RIXS spectra.

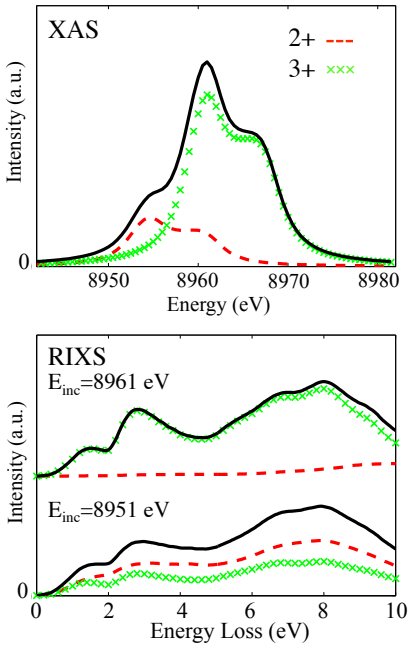

FIG. S2. (Color online) Calculated Yb L_3 XAS spectrum (top panel) and RIXS spectra for incident energies of 8951 eV and 8961 eV (bottom panel) decomposed into their Yb^{2+} and Yb^{3+} components.

same as $|g\rangle$, but in the final state of RIXS all eigenstates $|i'\rangle$, so that all final states $|f_{k_e,k_v,i'}\rangle$ with energy $E_{k_e,k_v,i'}(= \epsilon_{5d_{k_e}} - \epsilon_{5d_{k_v}} + E_{i'})$, can contribute to the RIXS spectra, because of the non-orthogonality between $|i\rangle$ and $|i'\rangle$. The RIXS spectra are given by

$$F_{\rm RIXS}(\Omega,\omega) = \sum_{k_e,k_v,i'} \left| \sum_i \frac{\langle f_{k_e,k_v,i'}|M'|m_{k_e,i}\rangle\langle m_{k_e,i}|M|g\rangle}{E_g+\Omega-E_{k_e,i}+{\rm i}\Gamma} \right|^2 \times G(E_{k_e,k_v,i'}+\omega-E_g-\Omega), \quad \text{(S8)}$$

where M' is the one-electron dipole-transition operator from $5d$ (below the Fermi level) to $2p_{3/2}$ states, ω is the emitted photon energy, and $G(x)$ is the Gaussian function with the central energy at x =0 and with the full width at half maximum 0.2 eV. In the calculation of the RIXS spectra, we disregard the interference effect, for simplicity.

Since the $5d$ electrons do not interact with other electrons, each intermediate state (as well as each final state) of RIXS is simply given by a direct product of two sub-systems, the non-interacting $5d$ and $2p_{3/2}$ electrons system and the many-body system consisting of the coupled $4f$ and ligand electrons including the core hole potential (in the intermediate state). The transition paths for the many-body system is illustrated in Fig. 2(b), where the transition probabilities are given by $|\langle i|g\rangle|^2$ and $|\langle i'|i\rangle|^2$ for the excitation and de-excitation processes. On the other hand the transition paths for the non-interacting electrons system are evident, and the spectra of XAS and RIXS are proportional to the DOS of the $5d$ electron above the Fermi level and the joint DOS of the $5d$ electron-hole excitations. Therefore, the XAS spectrum is given by the convolution of the many-body spectral function (DOS of intermediate states $|i\rangle$ weighted by the transition probability $|\langle i|g\rangle|^2$ for each Ω) and the $5d$ electron DOS, as shown in Fig. 2(b). In the same way, the RIXS spectrum is given by the spectral function of the many-body system and the joint DOS of $5d$ electron-hole pair excitations. The good agreement between the calculated and measured XAS spectrum and incident energy dependence of the RIXS spectra is illustrated in Figure S1.

As indicated by Eqs.(S6) and (S7), each final state $|f_{k_e,k_v,i'}\rangle$ is the mixed state of the $4f^{14}$ (Yb^{2+}) and $4f^{13}c$ (Yb^{3+}) configurations. However, if we can choose the transition paths only through the $\underline{2p_{3/2}}5d4f^{14}$ intermediate state, the contribution from the Yb^{2+} configuration to the RIXS spectrum will be separated out because of the transition probability $|\langle i'|i\rangle|^2$. Actually by tuning the incident photon energy at the Yb^{2+} satellite structure of XAS, we can select the intermediate states with more $\underline{2p_{3/2}}5d4f^{14}$ weight than the $\underline{2p_{3/2}}5d4f^{13}c$ weight, although the two configurations are superposed with each other in the intermediate state due to the lifetime broadening by the core hole (see the XAS spectrum in Fig. 2(b) and Fig. S2). Therefore, we can control the contributions from the Yb^{2+} and Yb^{3+} configurations to the RIXS

spectrum by choosing the incident energy, as shown in the RIXS spectra in Fig. 2(b) and Fig. S2. If we take into account the Coulomb interaction between $4f$ and $5d$ electrons, which is disregarded in the present calculations, the joint DOS of $5d$ electron-hole pair excitations will be different for Yb^{2+} and Yb^{3+} configurations, and the difference will be detected by utilizing the resonance effect in RIXS. In this paper we succeeded in measuring such a difference by the RIXS experiment.

[S1] A. Kotani, Eur. Phys. J. B **85**, 31 (2012).

[S2] A. Kotani, K. O. Kvashinina, P. Glatzel, J. C. Parlebas, and G. Schmerber, Phys. Rev. Lett. **108**, 036403 (2012).

[S3] A. Kotani, K. O. Kvashinina, S. M. Butorin, and P. Glatzel, Eur. Phys. J. B **85**, 257 (2012).

[S4] A. Kotani, Mod. Phys. Letters B **27**, 1330012 (2013).

[S5] V. N. Antonov, M. Galli, F. Marabelli, A. N. Yaresko, A. Ya. Petrov, and E. Bauer, Phys. Rev. B **62**, 1742 (2000).

[S6] O. Gunnarsson and K. Schönhammer, Phys. Rev. B **28**, 4315 (1983).